nature neuroscience

Identification of a cellular node for motor control pathways

Ariel J Levine[1–3], Christopher A Hinckley[1–3], Kathryn L Hilde[1,2], Shawn P Driscoll[1,2], Tiffany H Poon[1,2], Jessica M Montgomery[1,2] & Samuel L Pfaff[1,2]

The rich behavioral repertoire of animals is encoded in the CNS as a set of motorneuron activation patterns, also called 'motor synergies'. However, the neurons that orchestrate these motor programs as well as their cellular properties and connectivity are poorly understood. Here we identify a population of molecularly defined motor synergy encoder (MSE) neurons in the mouse spinal cord that may represent a central node in neural pathways for voluntary and reflexive movement. This population receives direct inputs from the motor cortex and sensory pathways and, in turn, has monosynaptic outputs to spinal motorneurons. Optical stimulation of MSE neurons drove reliable patterns of activity in multiple motor groups, and we found that the evoked motor patterns varied on the basis of the rostrocaudal location of the stimulated MSE. We speculate that these neurons comprise a cellular network for encoding coordinated motor output programs.

Common movements, such as reaching and grasping an object or stepping, involve complex neural calculations to select the appropriate muscles and precisely control the timing of their contractions to achieve the desired outcome. This motor coordination involves many regions in the central nervous system (CNS), including the motor cortex, red nucleus, basal ganglia, brainstem, cerebellum, peripheral sensory system and spinal neurons. These neural pathways ultimately converge onto motorneuron pools that are each dedicated to controlling a single muscle of the body. Given the number of muscles and possible joint positions of the body that can vary at each moment, the efficiency and reliability of common movements are remarkable.

To simplify the motor-control tasks of the CNS, neural plans for compound movements that invoke multiple joints or body regions are thought to be fractionated into a series of subroutines or 'synergies' that bind together useful combinations of motorneuron activation[1–3]. These synergies may then be flexibly recruited into multiple types of movement, such as voluntary and reflexive behaviors. It has long been recognized that voluntary movements and those evoked by direct stimulation of the motor cortex have similarities with movements activated by sensory reflexes[4–7]. Because the cortex and peripheral nervous system have direct connections into the spinal cord, we tested whether these inputs converge onto a shared spinal motor circuitry for coordinating motor actions. We identified a spatially and molecularly defined population of neurons in the deep dorsal horn of the spinal cord that are candidates to encode the programs for motor synergies; this population comprises a network of neurons at the point of intersection between the corticospinal and sensory pathways. Because activation of these neurons is sufficient to elicit reliable and coordinated motorneuron activity, we designated these cells motor synergy encoder (MSE) neurons. Functional studies of MSE neurons revealed an orderly circuit organization, which we speculate helps to simplify the selection of the appropriate programs that underlie complex motor actions for purposeful movements.

RESULTS

A premotor neuron column in lamina V

Motor synergies that involve multiple hindlimb joints typically employ motor pools that are present in different lumbar (L) segments. For example, the stance phase of locomotion involves coextension by quadriceps motor pools in L2–3 and gastrocnemius motorneurons in L4–5 (refs. 8–10). To identify spinal neurons that may mediate coordination of motorneuron activity, we searched for intersegmentally projecting neurons with strong direct connections to motorneurons. We used a monosynaptic circuit–tracing strategy that limits the spread of trans-synaptic rabies virus to only first-order premotor neurons. This approach is based on co-infecting motorneurons with genetically modified rabies virus (RabΔG) and adeno-associated virus (AAV) encoding glycoprotein (AAV:G)[11,12]. Experiments were performed on mice between postnatal days 0–15 (P0–P15) because this time window provides the most efficient trans-synaptic labeling, with a minimum of neuronal toxicity, and because the distribution of premotor neurons is similar between pups and adults[13,14].

RabΔG and AAV:G were co-injected into a range of muscles that control joint movements of the hindlimb and forelimb. We studied the medial and lateral gastrocnemius muscles (ankle extensors), the tibialis anterior (ankle flexor), the quadriceps (knee extensor), the hamstrings (knee flexor), the wrist extensors, the wrist flexors, the triceps (elbow extensor) and the biceps (elbow flexor). We observed a dense column of ipsilateral neurons in the deep dorsal horn extending the length of the lumbar spinal cord for hindlimb muscles or the cervical spinal cord for forelimb muscles (n = 89 spinal cords; **Fig. 1a–c**,

[1]Gene Expression Laboratory, Salk Institute for Biological Studies, La Jolla, California, USA. [2]Howard Hughes Medical Institute, Salk Institute for Biological Studies, La Jolla, California, USA. [3]These authors contributed equally to this work. Correspondence should be addressed to S.L.P. (pfaff@salk.edu).

Received 4 February; accepted 13 February; published online 9 March 2014; doi:10.1038/nn.3675

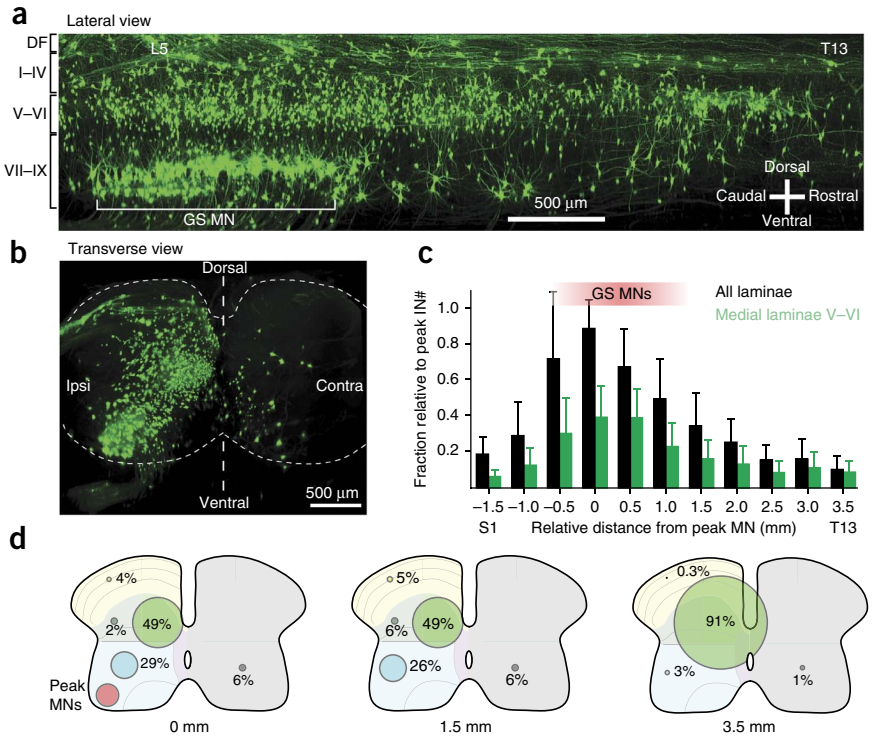

Figure 1 Labeling of first-order spinal neurons targeting gastrocnemius motorneurons. (**a**,**b**) Images of a RabΔG:GFP-labeled spinal cord following injection into the medial gastrocnemius (GS) muscle. (**a**) Lateral projection of an optically cleared lumbar spinal cord, shows motorneurons (GS MNs) in the ventral horn of L4 and L5 spinal segments. Premotor cells and fibers can be seen in the dorsal funiculus (DF), laminae I–IV, laminae V–VI and laminae VII–IX. (**b**) Collapsed transverse view of the lumbar spinal cord in **a**, shows ipsilateral (ipsi) and contralateral (contra) premotor cells. (**c**) Quantification of total pregastrocnemius spinal neurons (all laminae) and of the subset of pregastrocnemius neurons in medial laminae V–VI along the rostral-caudal axis of the lumbar spinal cord. Neuron counts (IN#) were normalized to the maximum number of neurons in a single section for each spinal cord to control for the variability in labeling. Means and s.d. are shown. Values are listed in **Supplementary Table 1**. Location 0 indicates the section with the peak number of motorneurons, and is usually in caudal L4. (**d**) Premotor cell distributions depicted on transverse spinal cord images representing the spinal level with peak motorneurons (0 mm), at a level 1.5 mm rostral (mid-lumbar) and at a level 3.5 mm rostral (upper lumbar/lower thoracic). Laminae were divided into functional regions, and the percentage of total premotor cells at each level are shown for each region, represented by the diameter of the colored circles. These regions are superficial dorsal horn (laminae I–IV, yellow), medial deep dorsal horn (medial laminae V–VI, green), lateral deep dorsal horn (lateral laminae V–VI, gray), ventral horn (laminae VII–IX, blue) and contralateral (gray).

Supplementary Figs. 1 and **2**, and data not shown). The cell bodies of this column were predominantly concentrated in medial lamina V, but we also observed sparse cell labeling in lateral lamina V and medial laminae IV and VI (**Fig. 1b–d** and **Supplementary Figs. 1** and **2**). To determine whether the premotor neurons in laminae IV–VI were a unique subset of cells or representative of typical neurons in this region of the spinal cord, we examined their morphology in spinal cords with sparse premotor trans-synaptic RabΔG labeling to better identify individual cells. The laminae IV–VI premotor neurons had large cell bodies (10–30 µm) and dendritic morphologies typical of Golgi-labeled laminae IV–VI neurons[15], which suggested that the premotor neurons were representative of the general population of neurons in the deep dorsal horn rather than a unique morphological cell type (**Supplementary Fig. 1**).

Trans-synaptic labeling revealed the processes of these deep dorsal horn premotor cells to be within a dense cluster centered in medial lamina V. Axons of these cells entered the ventrolateral white matter and cornu-commissuralis of Marie in the dorsal funiculus (**Supplementary Fig. 1a**), which are known tracts for intersegmentally projecting axons[15,16]. Consistent with this intersegmental axonal labeling pattern, we detected premotor neurons up to eight spinal cord segments from their motorneuron targets (**Fig. 1a**,**c**,**d** and data not shown).

To quantify distributions of premotor neurons, we selected a single muscle, the ankle extensor gastrocnemius, and analyzed its premotor circuitry by regional and laminar distribution[17]. 52% of all rabies virus–labeled pregastrocnemius spinal neurons were located in the medial deep dorsal horn (laminae V–VI), compared with 28% in the ipsilateral ventral horn (laminae VII–IX), 7% in the contralateral spinal cord, 4% in the superficial dorsal horn (laminae I–IV) and 3% in the lateral deep dorsal horn (laminae V–VI) (n = 4,594 cells in 20 spinal cords; **Fig. 1b–d**). The fraction of total premotor spinal neurons that were located in the medial deep dorsal horn increased at progressively rostral levels, reaching over 90% in upper lumbar and lower thoracic levels (**Fig. 1c**,**d** and **Supplementary Table 1**).

These viral tracing studies revealed a column of premotor spinal neurons for a variety of motor pools located in the medial area of the deep dorsal horn, consistent with previous studies that identified premotor and putative premotor spinal neurons using a wide range of techniques[12–14,18–22]. Medial deep dorsal horn premotor neurons are notable because they quantitatively represent the most prominent source of rabies virus–identified monosynaptic input onto motorneurons, extend axons across multiple spinal cord segments and are in the deep dorsal horn of the spinal cord, a region that is sufficient to drive motor synergies after electrical stimulation[23].

Premotor lamina V neurons bind the activity of multiple motor pools

We hypothesized that rabies-labeled premotor neurons concentrated in medial lamina V were cellular candidates to mediate motor synergies for multijoint movements. To explore this possibility, we tested whether direct activation of these neurons was sufficient to evoke reliable and coordinated motorneuron activity in the functionally related motor groups of the L2 and L5 spinal segments. This provides a simple model of a motor synergy. We used monosynaptic rabies-virus tracing to deliver the light-activated cation channel channelrhodopsin 2 (RabΔG:ChR2)[24] to pregastrocnemius neurons, exposed the medial surface of the spinal cord and delivered focal, short-duration pulses of light to directly excite the pregastrocnemius medial deep dorsal horn neurons (**Fig. 2a**). To analyze motor activity, we performed electrical recordings of the L5 ventral root, which includes gastrocnemius motorneuron axons, and the L2 ventral root, which contains the motorneuron axons of the functionally

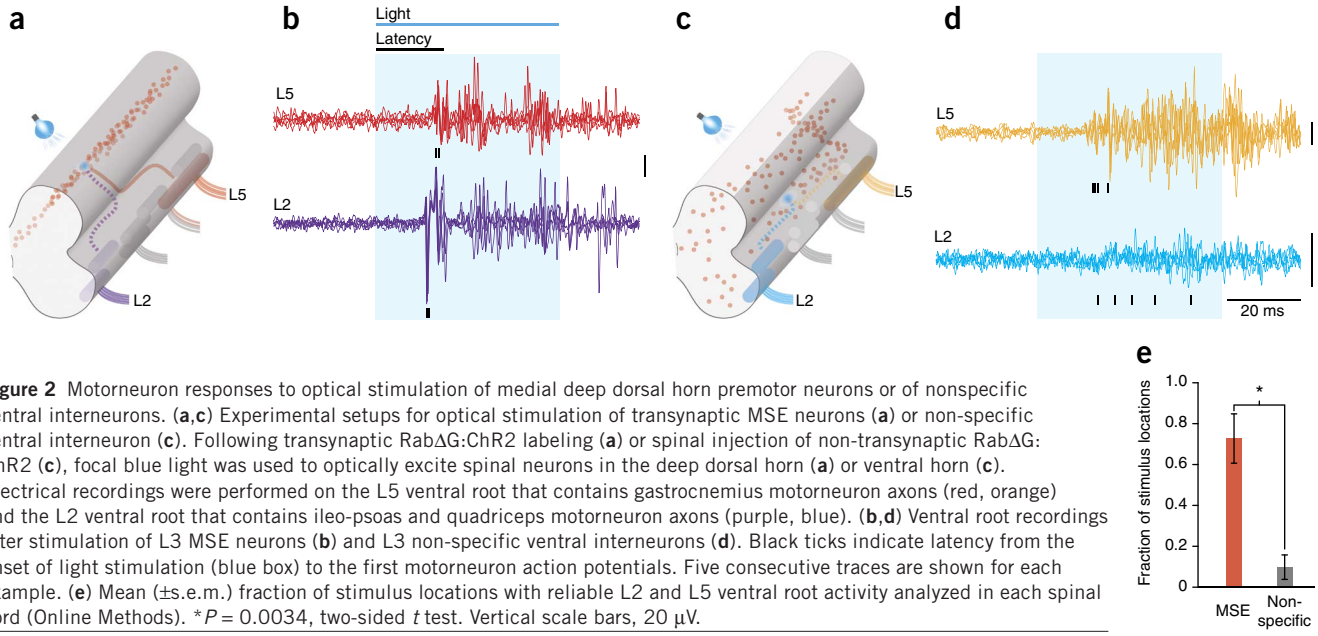

Figure 2 Motorneuron responses to optical stimulation of medial deep dorsal horn premotor neurons or of nonspecific ventral interneurons. (**a**,**c**) Experimental setups for optical stimulation of transynaptic MSE neurons (**a**) or non-specific ventral interneuron (**c**). Following transynaptic RabΔG:ChR2 labeling (**a**) or spinal injection of non-transynaptic RabΔG:ChR2 (**c**), focal blue light was used to optically excite spinal neurons in the deep dorsal horn (**a**) or ventral horn (**c**). Electrical recordings were performed on the L5 ventral root that contains gastrocnemius motorneuron axons (red, orange) and the L2 ventral root that contains ileo-psoas and quadriceps motorneuron axons (purple, blue). (**b**,**d**) Ventral root recordings after stimulation of L3 MSE neurons (**b**) and L3 non-specific ventral interneurons (**d**). Black ticks indicate latency from the onset of light stimulation (blue box) to the first motorneuron action potentials. Five consecutive traces are shown for each example. (**e**) Mean (±s.e.m.) fraction of stimulus locations with reliable L2 and L5 ventral root activity analyzed in each spinal cord (Online Methods). *$P = 0.0034$, two-sided t test. Vertical scale bars, 20 μV.

related muscles: the quadriceps and ileo-psoas hip flexors. Quadriceps activity is coordinated with gastrocnemius activity during the stance phase of locomotion[10] and the ileo-psoas has been reported to be activated with the gastrocnemius in specific cases of the pain-withdrawal reflex[25–27]. We considered that optical stimulation of gastrocnemius premotor neurons would drive only L5 electrical activity if these neurons control only the gastrocnemius motor pool or would drive dual L2 and L5 activity if these neurons control coordinated activity of motor groups for multiple joints.

We found that optical stimulation of medial deep dorsal horn pre-gastrocnemius neurons evoked detectable motorneuron responses in both the L5 ventral root (10/10 spinal cords) and the L2 ventral root (9/10 spinal cords) (**Fig. 2b**). We analyzed spinal cords that met our minimum criteria for efficiency of labeling with rabies virus (Online Methods) by performing optical stimulations in sets of ten trials over a range of stimulation locations from L1 to L6. Among this set, we found that all stimulation locations produced some motor response, but 72.7 ± 0.2% (mean ± s.d.) of premotor medial deep dorsal horn stimulation locations produced dual L2 and L5 motorneuron activity without any trial failures ($n = 78$ locations in four spinal cords, with ten trials at each location; **Fig. 2e**). These data show that first-order premotor medial deep dorsal horn neurons have reliable and functional outputs capable of activating multiple motor groups.

Taken together, these findings reveal a population of spinal neurons that have four key features related to motor synergies. First, these neurons represent a major source of the direct synaptic input to motorneurons. Second, they extend axons intersegmentally and therefore are well-suited to bind spatially segregated but functionally related motor pools. Third, these cells are located in the deep dorsal horn, the region from which electrical stimulation of the spinal cord can best evoke motor synergies[23]. Finally, direct stimulation of these cells is a sufficient and reliable means to activate multiple motor groups. Accordingly, we considered that these cells are candidates to be motor synergy encoders, and we designated them MSE neurons.

Features of MSE neuron–evoked motor responses

We sought to determine the specific features of motorneuron activity evoked by candidate MSE neurons by comparison with motor responses driven by other classes of spinal neurons. To provide a control group of spinal interneurons with which to compare MSE cell function, it was necessary to achieve comparable levels of ChR2 expression in a comparable number of cells but in an unbiased set of spinal interneurons. We performed intraspinal injections of replication-defective RabΔG:ChR2 to infect spinal neurons at L4 or L5 as well as the intersegmental neurons that project to these levels and take up the RabΔG:ChR2 at their terminals ($n = 7$ spinal cords; **Fig. 2c**). We performed these experiments without complementing glycoprotein, to restrict RabΔG:ChR2 expression to initially infected neurons following intraspinal injection. We then performed optical excitation experiments over the ventral spinal cord, to probe the effects of nonspecific ventral interneurons on L2 and L5 motor activity.

We found that optical stimulation of nonspecific ventral interneurons evoked some detectable motor response from all stimulation locations, which is consistent with the known motor function of the ventral spinal cord ($n = 54$ locations in seven spinal cords; for example, **Fig. 2d**). However, only 8.3 ± 1.4% of stimulation locations evoked reliable dual L2 and L5 motor responses (mean and s.d.). This is in marked contrast with the 72.7% of MSE stimulation trials (two-sided t test, $P = 0.0034$; **Fig. 2e**). Thus, although multiple classes of spinal neurons contribute to motor control in behavior, direct optical excitation of a broad and unbiased set of ventral spinal interneurons does not consistently evoke dual L2 and L5 motor group responses.

Further comparison of motor responses evoked by MSE neurons and nonspecific spinal neurons revealed that MSE neurons drive more robust and reliable motorneuron activity. We analyzed multiple features of the motor responses, such as the variability in the timing of the first spike and the percentage of trials that produced a motor response (Online Methods). Principal component analysis identified a general reliability component that encompassed each of these features, PC1 (**Supplementary Fig. 3**). This component was positively associated with MSE neuron–evoked motor activity of both the L5 and L2 ventral roots, and this was significant relative to the negative association of PC1 with responses evoked by stimulating the nonspecific set of ventral interneurons ($P = 0.010$ for L2 and $P = 0.024$ for L5, two-sided t test; **Supplementary Fig. 3**). This signature of reliability that characterizes motor activity evoked by MSE neurons demonstrates

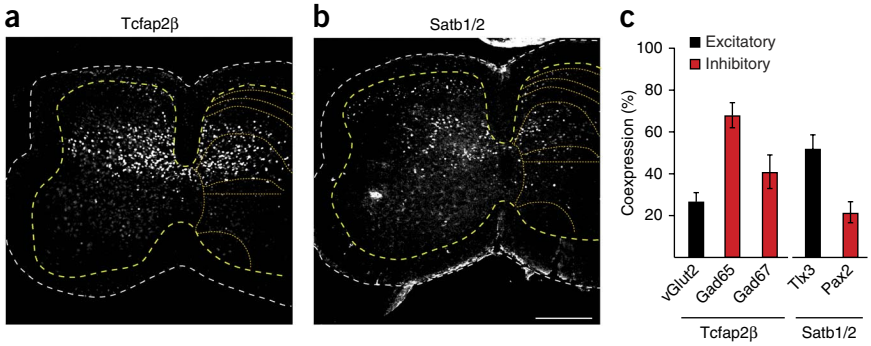

Figure 3 Molecular markers Tcfap2β and Satb1/2 identify medial deep dorsal horn neurons. (**a**,**b**) Projected confocal stacks showing immunolabeling of Tcfap2β (**a**) and Satb1/2 (**b**) in transverse sections of P8 lumbar spinal cord. Scale bar, 250 µm. (**c**) Neurotransmitter status of Tcfap2β and Satb1/2 cells determined using *in situ* hybridization at P10 against vGlut2 (excitatory), Gad65 (inhibitory), and Gad67 (inhibitory), or with antibodies at P2 to identify Tlx3 (excitatory) and Pax2 (inhibitory). Mean percentages ± s.d. are: 26 ± 4% of Tcfap2β$^+$ neurons expressed vGlut2 (n = 570 neurons in five P10 spinal cords), 67 ± 6% of Tcfap2β$^+$ neurons expressed Gad65 (n = 344 neurons in 4 P10 spinal cords) and 40 ± 8% expressed Gad67 (n = 201 neurons in three P10 spinal cords). It is likely that Gad65 and Gad67 are coexpressed in some cells. Among the Satb1/2$^+$ population, 22 ± 5% of all Satb1/2$^+$ expressed Pax2 (n = 1,056 neurons in 4 P2 spinal cords, mostly in the ventral subdivision of Satb1/2$^+$ medial deep dorsal neurons), and 52 ± 7% of all Satb1/2$^+$ expressed Tlx3 (n = 956 neurons in 4 P2 spinal cords, mostly in the dorsal subdivision of Satb1/2$^+$ medial deep dorsal horn neurons).

that this population has functional, high-fidelity outputs to multiple groups of motorneurons.

We next considered that the reliability of the dual motor responses may be explained by individual MSE neurons that contact multiple motorneuron pools through monosynaptic connections. To probe whether MSE neurons directly contact multiple motor pools, we performed two-color RabΔG:Cherry and RabΔG:GFP labeling experiments to visualize cells in the premotor circuitries of two muscles simultaneously. Although we observed doubly labeled (yellow) premotor cells for pairs of muscles that are commonly co-recruited during behavior, their infrequency suggests that they represent a minor portion of the paths by which MSE neurons access motorneurons (13/389 premedial gastrocnemius neurons, n = 6 spinal cords; **Supplementary Fig. 4**). The very low fraction that we observed may be an experimental underestimate owing to additive inefficiencies of two RabΔG viruses, but independent studies confirm that dual-labeled premotor cells represent a small fraction of the total premotor population[12,21].

These labeling studies suggested that MSE neurons likely use indirect connections to coordinately regulate multiple motor groups via polysynaptic pathways. This is supported by our measurements of the relatively long latencies to the first motorneuron spikes after optical stimulation of MSE neurons (for example, **Fig. 2b**). This polysynaptic transmission could be mediated by other neuron classes, but the relative unreliability of ventral interneuron-evoked dual L2 and L5 responses (**Fig. 2d**,**e** and **Supplementary Fig. 3**) suggests that this possibility is not sufficient to explain the reliable MSE neuron–evoked responses that we observed (**Fig. 2b**,**e** and **Supplementary Fig. 3**). Alternatively, MSE neurons may contact multiple groups of motorneurons through an interconnected MSE neuron network that enhances the robustness and reliability of motor responses, despite its polysynaptic path.

To determine whether candidate MSE neurons synaptically contact each other, we analyzed spinal cords in which medial gastrocnemius MSE neurons were labeled with RabΔG:Cherry and lateral gastrocnemius MSE neurons were labeled with RabΔG:GFP. In the medial deep dorsal horn, we observed dense Cherry$^+$ processes and GFP$^+$ processes surrounding MSE neurons labeled with both fluorescent proteins (**Supplementary Fig. 5**). We performed immunofluorescence assays to identify excitatory (vGlut2$^+$) and inhibitory (Gad67$^+$ or GlyT2$^+$) MSE GFP$^+$ synaptic terminals that overlapped with the Cherry$^+$ cell bodies (and vice versa). We found examples of both excitatory and inhibitory MSE-to-MSE neuron connectivity (**Supplementary Fig. 5**), which provides a potential pathway for MSE neurons to indirectly coordinate motorneuron responses via other MSE neurons. Thus, MSE neurons likely target multiple motorneuron groups through a combination of direct monosynaptic connections to multiple motorneuron pools and indirect connections through a polysynaptic MSE neuron network.

A molecular description of MSE cells

Having studied the connectivity and functional features of MSE neurons, we next began to characterize their cellular identity. To identify markers of the MSE cell population, we systematically screened the Gensat expression database[28] and cross-referenced these results with the Allen Brain Institute expression database[29]. We identified three candidate genes that are expressed in the medial deep dorsal horn at embryonic and postnatal stages, the transcription factor *Tfap2b* (also known as *Tcfap2β*) and the nuclear and chromatin organization factors *Satb1* and *Satb2* (refs. 30,31). Tcfap2β is expressed at late embryonic and early postnatal stages across lamina V (with overlap into laminae IV and VI) and in a few scattered cells in the ventral horn (**Fig. 3a**). We studied Satb1 and Satb2 together (Satb1/2), using an antibody that recognizes both proteins. Satb1/2 were expressed at mid-late embryonic stages in a cluster of cells in medial lamina V/VI (data not shown), and through postnatal stages in medial lamina V/VI and lamina III (**Fig. 3b**).

We determined the neurotransmitter status of Tcfap2β$^+$ and Satb1/2$^+$ cells. We found that the Tcfap2β$^+$ subpopulation of MSE neurons comprises a minor excitatory subtype and a major inhibitory subtype (**Fig. 3c** and **Supplementary Fig. 6**). Among the Satb1/2$^+$ MSE neuron population, we found these cells could be subdivided into distinct dorsal and ventral subgroups on the basis of their protein expression profiles. Most of the Satb1/2$^+$ neurons in the ventral region of medial lamina V–VI expressed the inhibitory marker Pax2, whereas most of the Satb1/2$^+$ neurons in the dorsal area of medial lamina V–VI expressed the excitatory marker Tlx3 (**Fig. 3c** and **Supplementary Fig. 6**).

Next, we examined whether Tcfap2β and Satb1/2 are expressed by MSE cells using immunofluorescence analysis of spinal cords with RabΔG-labeled MSE neurons. Tcfap2β was expressed in 23 ± 12% and Satb1/2 were expressed in 13 ± 11% of all pregastrocnemius spinal neurons (mean ± s.d., n = 4,594 cells in 20 spinal cords; **Fig. 4**). This is in comparison with other previously reported markers of premotor neurons that account for 2.1% ($V0_c$ ChAT$^+$), 2.5% (dI3 Isl1$^+$), 3% (V2 Lhx3$^+$) and 3.4% (Renshaw calbindin$^+$) of premotor

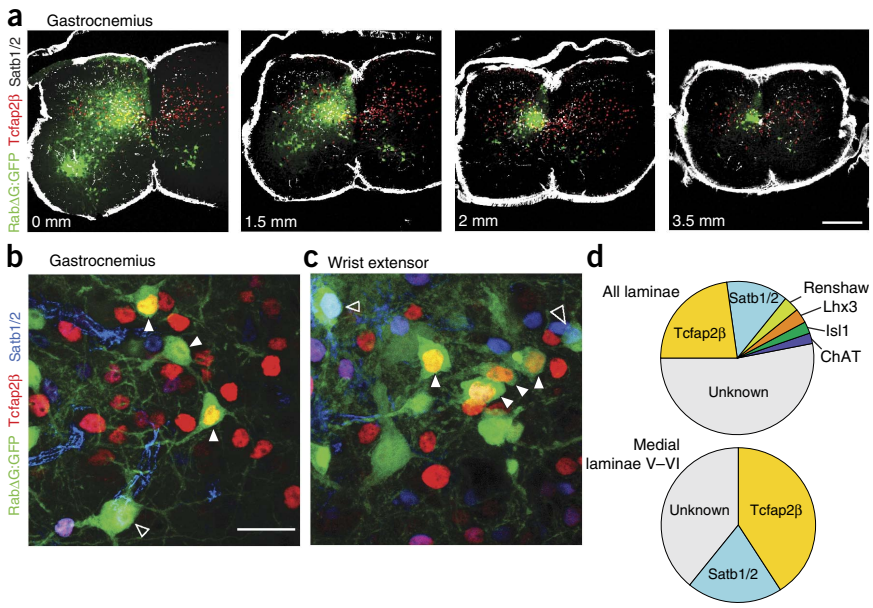

Figure 4 Molecular markers Tcfap2β and Satb1/2 identify medial deep dorsal horn premotor neurons. (**a**–**c**) Projected confocal stacks showing combined immunolabeling and RabΔG labeling in transverse sections of P8 lumbar spinal cords. Distribution of gastrocnemius motorneurons and pregastrocnemius spinal neurons (RabΔG:GFP) at four rostral-caudal levels, together with immunolabeling of Tcfap2β and Satb1/2 (white) (**a**). The levels are at the peak of gastrocnemius motorneurons (0 mm), and 1.5 mm, 2 mm and 3.5 mm rostral. Higher-magnification images of the RabΔG-labeled premotor spinal neurons in the medial deep dorsal horn (green), positive for Tcfap2β (yellow, filled arrowheads) and Satb1/2 (light blue, unfilled arrowheads), that are directly presynaptic to the gastrocnemius (**b**) or wrist extensors (**c**). (**d**) Fraction of total pregastrocnemius spinal neurons (top) and medial laminae V–VI premotor spinal neurons (bottom) identified by Tcfap2β, Satb1/2 and other previously described premotor spinal neuron classes[12,32]. Scale bars, 250 μm (**a**) and 25 μm (**b**,**c**).

spinal neurons[12,32]. In the medial deep dorsal horn, Tcfap2β antibody labeling identified 41 ± 17% and Satb1/2 labeling identified 20 ± 13% of pregastrocnemius neurons (mean ± s.d., n = 2,402 cells in 20 spinal cords; **Fig. 4d**). A small percentage of cells were positive for both Tcfap2β and Satb1/2 antibodies. We observed similar results in pre-tibialis anterior, pre-hamstrings, pre-quadriceps and pre-wrist extensor studies (**Fig. 4c** and **Supplementary Fig. 2**). These data provide, to the best of our knowledge, the first assignment of molecular markers to this population of premotor cells, reveal that MSE neurons are a heterogeneous population and suggest that the combination of medial deep dorsal horn cell location, together with Tcfap2β or Satb1/2 expression status can serve as a surrogate for identification of MSE neurons. Further studies will be needed to probe the functions of MSE neuron subpopulations.

MSE neurons receive sensory and corticospinal inputs

It has been shown that motor synergies can be activated by different neural pathways, including sensory reflexes and motor cortex stimulation[6,7,33,34]. This creates specific expectations for the types of inputs that MSE neurons should receive, namely, inputs from sensory pathways and from pyramidal cells in the motor cortex.

Proprioceptive sensory inputs may modulate motor synergies, cooperate with them to engage multiple motor pools or inform MSE cells about the position of the limb before initiation of movement. It is known that primary proprioceptive afferents have dense terminations in the medial deep dorsal horn[35,36], and we found that 98 ± 2% of MSE cells were contacted by proprioceptive parvalbumin$^+$ and vGlut1$^+$ terminals or *Parvalbumin::synaptophysin-tdTomato*$^+$ terminals (n = 84 cells in three spinal cords; **Fig. 5a**,**d**). We then analyzed a set

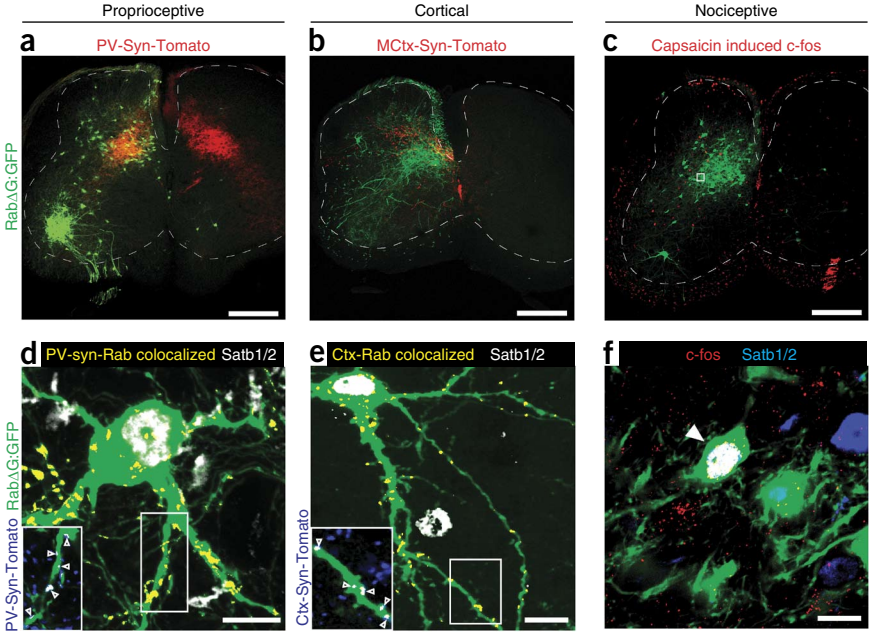

Figure 5 MSE neurons receive sensory and corticospinal inputs. (**a**) RabΔG labeling of pregastrocnemius MSE (green) and genetic labeling of proprioceptive afferent synaptic terminals (*Parvalbumin::synaptophysin-tdTomato* (PV-Syn-Tomato), red). (**b**) RabΔG labeling of pre-tibialis anterior (TA) MSE (green) and genetic labeling of corticospinal terminations from the caudal motor cortex, following focal unilateral injection of AAV:Cre into the caudal motor cortex of cre-dependent *synaptophysin-tdTomato* (MCtx-Syn-Tomato, red) pups. (**c**) RabΔG labeling of MSE and immunolabeled capsaicin induced c-fos expression. (**d**,**e**) To stringently identify synaptic inputs onto RabΔG:GFP$^+$ (green) and Satb1/2$^+$ (white) MSE neurons from *Parvalbumin::synaptophysin-tdTomato* (**d**) or *Emx1::synaptophysin-tdTomato* (Ctx-Syn-Tomato) (**e**) neurons, colocalized GFP$^+$ and Tomato$^+$ pixels were identified, pseudocolored yellow and projected onto the GFP$^+$ neuron. As a result of this analysis, Syn-Tomato that was not colocalized with the GFP$^+$ neuron is not shown. Insets show single optical slices and also depict the total Syn-Tomato (blue) so that sites of synaptic contacts appear white. (**f**) High-magnification projected confocal image of a RabΔG-pre-TA (green)/Satb1/2$^+$ (blue) MSE neuron boxed in **c** activated by a painful heel stimulus (c-fos, red), arrowhead. Scale bars, 250 μm (**a**–**c**) and 10 μm (**d**–**f**).

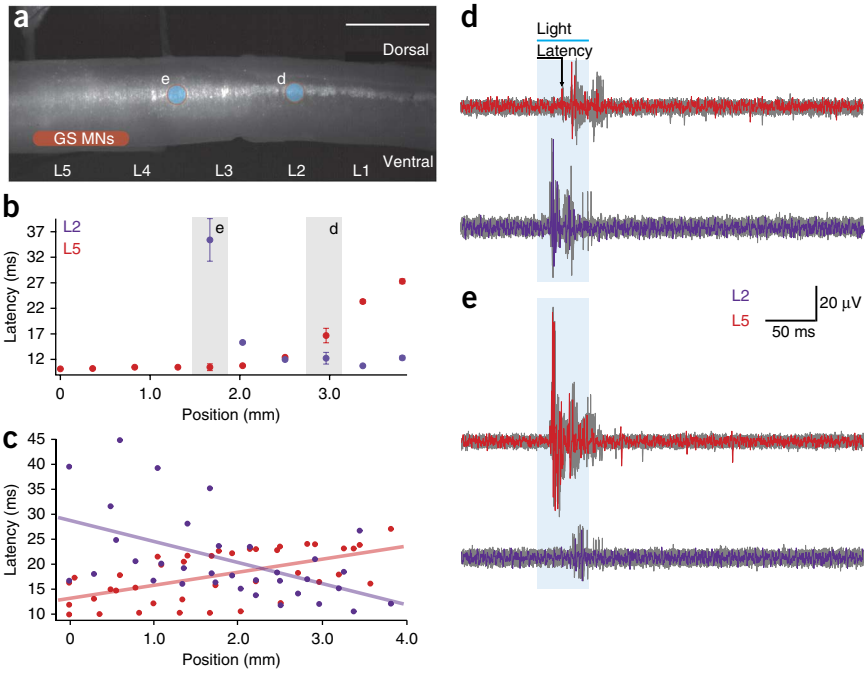

Figure 6 Rostral-caudal position of MSE neurons maps to distinct functional outputs. (**a**) Stereoscope image of the medial surface of a P8 lumbar spinal cord revealing the MSE column in the medial deep dorsal horn, labeled by pre-gastrocnemius RabΔG:ChR2-Cherry. The approximate location of gastrocnemius motorneurons (GS MNs), lumbar segments (L1–L5) and stimulation sites for data in **d** and **e** (blue circles) are shown. Scale bar, 1 mm. (**b**,**c**) Average latency of the first action potentials in the L2 and L5 ventral roots in one spinal cord (**b**) and as composite data from four spinal cords (**c**) after optical stimulation at multiple locations along the rostral-caudal axis (position). Error bars, s.d. for 10 traces for each location in **b**. Locations and latency points for data in **d** and **e** are boxed in gray. 0 position represents the caudal end of L5. The relationships between latency and location in the composite data were fit with a linear model (lines in **c**). (**d**,**e**) L5 and L2 ventral root traces (representative single traces are shown in red (L5) or purple (L2) and individual traces are in gray) after optical stimulation (blue boxes) of pregastrocnemius medial deep dorsal neurons in the L2 spinal segment (**d**) and the L3–L4 border (**e**). For a full set of additional traces, see **Supplementary Figure 8**.

of premotor medial deep dorsal horn neurons that expressed Tcfap2β or Satb1/2 and found that 93.8% of these cells received proprioceptive synaptic contacts that we validated by co-localization of a genetic label of presynaptic terminals (*Parvalbumin::synaptophysin-tdTomato*) and the post-synaptic marker PSD95 (n = 30 cells in eight spinal cords; data not shown). The proprioceptive inputs onto premotor, marker-positive, medial deep dorsal horn cells were numerous, with 36 ± 7 contacts per cell (n = 8 cells in three spinal cords), and we observed these over the cell body and processes (26 ± 16% on cell bodies and 74 ± 16% on processes, mean ± s.d.; **Fig. 5d** and **Supplementary Fig. 7**).

To determine whether motor cortex projections via the corticospinal tract may direct motor commands using MSE neurons as intermediaries, we analyzed spinal cords at P14–15 when the corticospinal tract is relatively mature[37,38]. We used a new genetic strategy (*Emx1::synaptophysin-tdTomato*) to identify total corticospinal presynaptic terminals. We found that 93% of Tcfap2β$^+$ or Satb1/2$^+$ MSE cells received corticospinal synaptic contacts (n = 14 cells in seven spinal cords). We found multiple synaptic contacts on each positive cell (22.5 ± 18 contacts per cell, mean ± s.d.; **Fig. 5e**), with up to 65 contacts on a single cell. We found these synapses on both the cell bodies and the processes of MSE cells (22.7% of contacts on cell bodies and 77.3% of contacts on processes, n = 292 contacts on 13 cells in seven spinal cords), and on dendritic spines (**Fig. 5e** and **Supplementary Fig. 7**). It has previously been shown that the medial deep dorsal horn is the major target of the caudal motor cortex[39]. To determine specifically whether the caudal motor cortex has direct input onto candidate MSE cells, we performed focal injections of AAV:Cre into the caudal motor cortex of *lox-stop-lox:synaptophysin-tdTomato* mice and examined the spinal targets of labeled synapses. We observed synaptic terminals of the caudal motor cortex in the deep dorsal horn, overlapping with the region of MSE neurons (**Fig. 5b**) and directly contacting MSE cells (n = 16 contacts on nine cells in four spinal cords; data not shown).

We next characterized whether candidate MSE neurons are functionally recruited by nociceptive pathways. Although most primary nociceptive fibers terminate in the superficial dorsal horn, these neural signals are then relayed to the deep dorsal horn. Here they target multimodal neurons, including pain-withdrawal 'reflex encoder' neurons that translate noxious cutaneous signals into the appropriate single muscle reflex movements[40]. We found that a painful stimulus to the heel activated neurons in the superficial dorsal horn laminae I and II, and in the deep dorsal horn, where these neurons overlapped with Satb1/2$^+$ cells (**Fig. 5c**). In the deep dorsal horn, 71 ± 14% of c-fos$^+$ activated neurons expressed Satb1/2 (n = 247 cells in 11 spinal cords). In addition, we observed cells that were c-fos$^+$, Satb1/2$^+$ and directly premotor (**Fig. 5f**). Thus, MSE neurons are likely interposed in pain-withdrawal pathways and may encompass previously described 'reflex-encoder' neurons, serving to bind together smaller reflex modules.

Our findings demonstrate that putative MSE neurons receive inputs from sensory and cortical pathways, which places these cells in the networks that command multiple types of motor synergy–based movement. Thus, it is possible that MSE cells that receive both sensory and cortical inputs may represent the underlying cellular network for controlling motor programs common to reflex and voluntary motor behaviors.

Motor coordination programs map onto MSE neuron position

We found that MSE neurons for each motor pool form a longitudinal column that extends across many spinal segments. To determine whether unique information is encoded in the functional outputs of MSE neurons at different rostral-caudal levels, we optically stimulated the pregastrocnemius MSE column at focal sites from L1 to L6 and analyzed the onset latencies to the first motorneuron spikes in the L2 and L5 ventral roots (**Fig. 6a**). We found that stimulation of pregastrocnemius MSE neurons elicited motorneuron responses with spike latencies that varied reliably according to the optical excitation location. Specifically, the L5 latency increased at progressively rostral levels, whereas the L2 latency decreases at progressively rostral levels (n = 37 locations for L2 and 43 locations for L5, in four spinal cords; **Fig. 6b–e** and **Supplementary Fig. 8**). To determine to what extent

conduction delays contribute to this pattern, we analyzed conduction in the cornu-commisuralis of Marie after optical excitation of MSE neurons, and found that it was 1 ms mm^{-1}, which was significantly lower than the L5 slope of 2.6 ms mm^{-1} and the L2 slope of 4.2 ms mm^{-1} (confidence interval test, $P < 0.05$; see Online Methods and **Supplementary Fig. 9**). Thus, the conduction delay in MSE neurons contributes to, but does not account for, the distinct motorneuron activation patterns that we observed at different rostral-caudal MSE neuron stimulation sites.

Taken together, our findings suggest that spinal circuits for distinct motor outputs are arrayed in an orderly fashion along the rostral-caudal axis of the deep dorsal horn. This organizational feature may help to simplify the complex task of coordinating multiple muscles for purposeful movements by allowing sensory and cortical pathways to engage MSE neurons at defined rostral-caudal levels of the spinal cord to activate specific motor synergies.

DISCUSSION

We provide a circuit-based, spatial, molecular and functional characterization of a population of spinal neurons that are sufficient to trigger complex patterns of motor activity. We found that these cells uniquely combine the key features to mediate motor synergy programs as building blocks for both volitional and reflex motor behaviors (**Supplementary Fig. 10**). They are a major source of monosynaptic input to motorneurons. They can cross multiple spinal segments to reach target motorneurons, potentially linking spatially segregated but functionally related motorneuron pools. They are located in the medial deep dorsal horn, the region from which motor synergies are most efficiently evoked by electrical stimulation[23,41]. They drive reliable patterns of action potentials in multiple motorneuron pools in a reduced model of a motor synergy. They receive direct inputs from neural sources known to recruit motor synergies, such as sensory pathways and the corticospinal tract. Accordingly, we propose that these spinal neurons encode the motorneuron activation patterns for motor synergies, and we designate them MSE neurons.

In addition to MSE neurons, multiple interneuron classes in the spinal cord have important motor coordination function, particularly those ventral interneurons that make up the 'central pattern generator' (CPG) network that supports rhythmic locomotion and the embryonic lineage–defined classes that make up this network[32,42]. Direct activation of the CPG network drives patterns of motorneuron activation, and in this respect, the ventral CPG interneurons and MSE neurons are similar. However, we describe here that MSE neurons in the medial deep dorsal horn have the ability to coordinate motor activity and are major synaptic targets of the cortical and sensory pathways that can recruit motor synergies. Having identified MSE neurons as a key node in neural pathways for motor control, it is an important future direction to study the relationship between MSE neurons and the ventral locomotor circuitry.

Previous anatomical and physiological experiments provide strong support for the medial deep dorsal horn being an important site for motor control. This region is the major point of intersection of several important circuitry elements: the densest region of corticospinal fibers[21,38,39,43] and rubrospinal fibers[44–46], substantial multimodal sensory input including 'reflex-encoder' sensory relay neurons[40,47,48], and a major fraction of premotor neurons[12–14,18–22]. Functional experiments have demonstrated that spinal motor synergies are best evoked with electrical stimulation of the spinal cord from deep dorsal horn locations, even in spinal cords in which descending and sensory inputs have been removed[23,41]. Our data provide a medial deep dorsal horn cellular substrate for the neurons that control complex motor actions by forming a columnar network in which descending and sensory inputs can converge, and selected motor commands can be sent to multiple motor pools.

An intriguing observation from our work is the spatial arrangement in the MSE column, such that distinct motorneuron coordination patterns are encoded at different points along the rostral-caudal axis of the spinal cord. This finding is supported by previous observations that electrical stimulation of the spinal cord produces different movements of the hindlimb, depending on the rostral-caudal site of stimulation[23,41,49,50]. The spatial organization of the MSE column provides a simple axis for motor commands, such as the corticospinal tract, to target and direct diverse motor synergies. If the MSE column is a major path through which cortical information flows to motorneurons, the selection of spinal motor modules may be an important organizational strategy represented within the motor cortex. Indeed, recent work has described cortical maps of motor synergy recruitment after electrical stimulation[7,33,34].

It has been noted that grasping of an object resembles the palmar grasp reflex and that the swing phase of locomotion is related to the flexor withdrawal reflex. If the MSE neuron network first arose in simple animals lacking a motor cortex, perhaps the earliest functions of this network were related to mediating motor synergies of multijoint reflexes. The similarity of movements activated by volitional and reflex pathways suggests that as the cortex evolved, the corticospinal pathway may have coopted the existing MSE cell circuitry to likewise simplify the task of controlling complex multijoint movements. In spinal cord injury, spinal neuronal networks are effectively isolated from descending input, and volitional movement of the body is lost below the injury level. If motor synergies are autonomously encoded in spinal MSE neuron networks, perhaps in the same way evolution may have coopted this circuitry, it may be useful to target MSE cells for therapeutic intervention in order to facilitate purposeful movements in patients with spinal cord injury.

METHODS

Methods and any associated references are available in the online version of the paper.

Note: Any Supplementary Information and Source Data files are available in the online version of the paper.

ACKNOWLEDGMENTS

We acknowledge the generosity and advice of M. Goulding, R. Edgerton, A. Engmann, E. Callaway, J. Young, F. Osakada and F. Stam, P. Joshi and S. McConnell for instruction in cortical injections, and Q. Ma (Harvard Medical School, *in situ* probes) and C. Birchmeier (Max Delbruck Center for Molecular Medicine, Tlx3 antibody) for providing reagents. M. Sternfeld, M. Hayashi, K. Lettieri and Y. Bogoch provided support and advice. We thank R. Levine for his helpful reading of the manuscript. A.J.L. was supported by George E. Hewitt Foundation for Medical Research and Christopher and Dana Reeve Foundation. C.A.H. was supported by a US National Research Service Award fellowship from US National Institutes of Health NINDS. K.L.H. is supported as a National Science Foundation Graduate Research Fellow. S.L.P. is supported as a Howard Hughes Medical Institute investigator and as a Benjamin H. Lewis chair in neuroscience. This research was supported by the National Institute of Neurological Disorders and Stroke (grant R37NS037116), the Marshall Foundation and the Christopher and Dana Reeve Foundation.

AUTHOR CONTRIBUTIONS

A.J.L. and S.L.P. conceived of the study. A.J.L., C.A.H. and S.L.P. designed the study and prepared the manuscript. A.J.L., C.A.H. and K.L.H. carried out the experiments. S.P.D. performed the statistical analysis. J.M.M. contributed to histology experiments. A.J.L. and T.H.P. prepared the rabies virus.

COMPETING FINANCIAL INTERESTS

The authors declare no competing financial interests.

1. Tresch, M.C., Saltiel, P., d'Avella, A. & Bizzi, E. Coordination and localization in spinal motor systems. *Brain Res. Rev.* **40**, 66–79 (2002).
2. Bizzi, E., Cheung, V.C., d'Avella, A., Saltiel, P. & Tresch, M. Combining modules for movement. *Brain Res. Brain Res. Rev.* **57**, 125–133 (2008).
3. Duysens, J., De Groote, F. & Jonkers, I. The flexion synergy, mother of all synergies and father of new models of gait. *Front. Comput. Neurosci.* **7**, 14 (2013).
4. Sherrington, C.S. *The Integrative Action of the Nervous System* (C. Scribner's Sons, 1906).
5. Lundberg, A. Supraspinal control of transmission in reflex paths to motoneurones and primary afferents. *Prog. Brain Res.* **12**, 197–221 (1964).
6. Leyton, S. & Sherrington, C.S. Observations on the excitable cortex of the chimpanzee, orang-utan and gorilla. *Q. J. Exp. Physiol.* **11**, 135–222 (1917).
7. Graziano, M.S., Taylor, C.S. & Moore, T. Complex movements evoked by microstimulation of precentral cortex. *Neuron* **34**, 841–851 (2002).
8. McHanwell, S. & Biscoe, T.J. The localization of motoneurons supplying the hindlimb muscles of the mouse. *Phil. Trans. R. Soc. Lond. B* **293**, 477–508 (1981).
9. Nicolopoulos-Stournaras, S. & Iles, J.F. Motor neuron columns in the lumbar spinal cord of the rat. *J. Comp. Neurol.* **217**, 75–85 (1983).
10. de Leon, R., Hodgson, J.A., Roy, R.R. & Edgerton, V.R. Extensor- and flexor-like modulation within motor pools of the rat hindlimb during treadmill locomotion and swimming. *Brain Res.* **654**, 241–250 (1994).
11. Wickersham, I.R., Finke, S., Conzelmann, K.K. & Callaway, E.M. Retrograde neuronal tracing with a deletion-mutant rabies virus. *Nat. Methods* **4**, 47–49 (2007).
12. Stepien, A.E., Tripodi, M. & Arber, S. Monosynaptic rabies virus reveals premotor network organization and synaptic specificity of cholinergic partition cells. *Neuron* **68**, 456–472 (2010).
13. Coulon, P., Bras, H. & Vinay, L. Characterization of last-order premotor interneurons by transneuronal tracing with rabies virus in the neonatal mouse spinal cord. *J. Comp. Neurol.* **519**, 3470–3487 (2011).
14. Ruigrok, T.J., Pijpers, A., Goedknegt-Sabel, E. & Coulon, P. Multiple cerebellar zones are involved in the control of individual muscles: a retrograde transneuronal tracing study with rabies virus in the rat. *Eur. J. Neurosci.* **28**, 181–200 (2008).
15. Scheibel, M.E. & Scheibel, A.B. Terminal axonal patterns in cat spinal cord. II. The dorsal horn. *Brain Res.* **9**, 32–58 (1968).
16. Sherrington, C.S. & Laslett, E.E. Observations on some spinal reflexes and the interconnection of spinal segments. *J. Physiol. (Lond.)* **29**, 58–96 (1903).
17. Sengul, G., Puchalski, R.B. & Watson, C. Cytoarchitecture of the spinal cord of the postnatal (P4) mouse. *Anat. Rec.* **295**, 837–845 (2012).
18. Harrison, P.J., Jankowska, E. & Zytnicki, D. Lamina VIII interneurones interposed in crossed reflex pathways in the cat. *J. Physiol.* **371**, 147–166 (1986).
19. Hongo, T., Kitazawa, S., Ohki, Y. & Xi, M.C. Functional identification of last-order interneurones of skin reflex pathways in the cat forelimb segments. *Brain Res.* **505**, 167–170 (1989).
20. Puskar, Z. & Antal, M. Localization of last-order premotor interneurons in the lumbar spinal cord of rats. *J. Comp. Neurol.* **389**, 377–389 (1997).
21. Asante, C.O. & Martin, J.H. Differential joint-specific corticospinal tract projections within the cervical enlargement. *PLoS ONE* **8**, e74454 (2013).
22. Hongo, T., Kitazawa, S., Ohki, Y., Sasaki, M. & Xi, M.C. A physiological and morphological study of premotor interneurones in the cutaneous reflex pathways in cats. *Brain Res.* **505**, 163–166 (1989).
23. Tresch, M.C. & Bizzi, E. Responses to spinal microstimulation in the chronically spinalized rat and their relationship to spinal systems activated by low threshold cutaneous stimulation. *Exp. Brain Res.* **129**, 401–416 (1999).
24. Osakada, F. *et al.* New rabies virus variants for monitoring and manipulating activity and gene expression in defined neural circuits. *Neuron* **71**, 617–631 (2011).
25. Clarke, R.W. & Harris, J. The organization of motor responses to noxious stimuli. *Brain Res. Brain Res. Rev.* **46**, 163–172 (2004).
26. Pierrot-Deseilligny, E. & Burke, D. *The Circuitry of the Human Spinal Cord.* 350–352 (Cambridge University Press, 2012).
27. Schouenborg, J. & Kalliomaki, J. Functional organization of the nociceptive withdrawal reflexes. I. Activation of hindlimb muscles in the rat. *Exp. Brain Res.* **83**, 67–78 (1990).
28. Gong, S. *et al.* A gene expression atlas of the central nervous system based on bacterial artificial chromosomes. *Nature* **425**, 917–925 (2003).
29. Henry, A.M. & Hohmann, J.G. High-resolution gene expression atlases for adult and developing mouse brain and spinal cord. *Mammalian Genome* **23**, 539–549 (2012).
30. Wildner, H. *et al.* Genome-wide expression analysis of Ptf1a- and Ascl1-deficient mice reveals new markers for distinct dorsal horn interneuron populations contributing to nociceptive reflex plasticity. *J. Neurosci.* **33**, 7299–7307 (2013).
31. Britanova, O., Akopov, S., Lukyanov, S., Gruss, P. & Tarabykin, V. Novel transcription factor Satb2 interacts with matrix attachment region DNA elements in a tissue-specific manner and demonstrates cell-type-dependent expression in the developing mouse CNS. *Eur. J. Neurosci.* **21**, 658–668 (2005).
32. Alaynick, W.A., Jessell, T.M. & Pfaff, S.L. Snapshot: spinal cord development. *Cell.* **146**, 178 (2011).
33. Harrison, T.C., Ayling, O.G. & Murphy, T.H. Distinct cortical circuit mechanisms for complex forelimb movement and motor map topography. *Neuron* **74**, 397–409 (2012).
34. Ramanathan, D., Conner, J.M. & Tuszynski, M.H. A form of motor cortical plasticity that correlates with recovery of function after brain injury. *Proc. Natl. Acad. Sci. USA* **103**, 11370–11375 (2006).
35. Ishizuka, N., Mannen, H., Hongo, T. & Sasaki, S. Trajectory of group Ia afferent fibers stained with horseradish peroxidase in the lumbosacral spinal cord of the cat: three dimensional reconstructions from serial sections. *J. Comp. Neurol.* **186**, 189–211 (1979).
36. Scheibel, M.E. & Scheibel, A.B. Terminal patterns in cat spinal cord. 3. Primary afferent collaterals. *Brain Res.* **13**, 417–443 (1969).
37. Gianino, S. *et al.* Postnatal growth of corticospinal axons in the spinal cord of developing mice. *Brain Res. Dev. Brain Res.* **112**, 189–204 (1999).
38. Curfs, M.H., Gribnau, A.A. & Dederen, P.J. Selective elimination of transient corticospinal projections in the rat cervical spinal cord gray matter. *Brain Res. Dev. Brain Res.* **78**, 182–190 (1994).
39. Martin, J.H. Differential spinal projections from the forelimb areas of the rostral and caudal subregions of primary motor cortex in the cat. *Exp. Brain Res.* **108**, 191–205 (1996).
40. Schouenborg, J., Weng, H.R., Kalliomaki, J. & Holmberg, H. A survey of spinal dorsal horn neurones encoding the spatial organization of withdrawal reflexes in the rat. *Exp. Brain Res.* **106**, 19–27 (1995).
41. Saltiel, P., Tresch, M.C. & Bizzi, E. Spinal cord modular organization and rhythm generation: an NMDA iontophoretic study in the frog. *J. Neurophysiol.* **80**, 2323–2339 (1998).
42. Goulding, M. Circuits controlling vertebrate locomotion: moving in a new direction. *Nat. Rev. Neurosci.* **10**, 507–518 (2009).
43. Bareyre, F.M., Kerschensteiner, M., Misgeld, T. & Sanes, J.R. Transgenic labeling of the corticospinal tract for monitoring axonal responses to spinal cord injury. *Nat. Med.* **11**, 1355–1360 (2005).
44. Liang, H., Paxinos, G. & Watson, C. The red nucleus and the rubrospinal projection in the mouse. *Brain Struct. Funct.* **217**, 221–232 (2012).
45. Brown, L.T. Rubrospinal projections in the rat. *J. Comp. Neurol.* **154**, 169–187 (1974).
46. Antal, M. *et al.* The termination pattern and postsynaptic targets of rubrospinal fibers in the rat spinal cord: a light and electron microscopic study. *J. Comp. Neurol.* **325**, 22–37 (1992).
47. Lundberg, A. Multisensory control of spinal reflex pathways. *Prog. Brain Res.* **50**, 11–28 (1979).
48. Schomburg, E.D. Spinal sensorimotor systems and their supraspinal control. *Neurosci. Res.* **7**, 265–340 (1990).
49. Barthelemy, D., Leblond, H., Provencher, J. & Rossignol, S. Nonlocomotor and locomotor hindlimb responses evoked by electrical microstimulation of the lumbar cord in spinalized cats. *J. Neurophysiol.* **96**, 3273–3292 (2006).
50. Mushahwar, V.K., Aoyagi, Y., Stein, R.B. & Prochazka, A. Movements generated by intraspinal microstimulation in the intermediate gray matter of the anesthetized, decerebrate, and spinal cat. *Can. J. Physiol. Pharmacol.* **82**, 702–714 (2004).

ONLINE METHODS

Animals. The following strains of mice (male and female) were used: wild-type, *Emx1*$^{tm1(cre)Krj}$*/J* (Jax 005628) *Pvalb*$^{tm1(cre)Arbr}$*/J* (Jax 008069), *Gt(ROSA)26Sor*$^{tm34.1(CAG-Syp/tdTomato)Hze}$*/J* (Jax 012570) and a transgenic *Hb9:B19G* line that we generated. This last line was made using a DNA fragment with the *Hb9* promoter driving expression of the rabies B19G strain glycoprotein. We found that transgenic expression of B19G was inadequate for trans-synaptic rabies spread, so this line was used in a limited number of experiments, and AAV:G was used together with this line. All experiments were done in accordance with Institutional Animal Care and Use Committee animal protocols and BSL2+ safety protocols, on animals housed in groups on a 12-h light-dark cycle.

Virus preparation and injections. AAV2/6 containing a general promoter and the rabies B19G strain glycoprotein was produced by Applied Viromics at a titer of 1×10^{12}–3×10^{13} genome copies/ml. Rabies virus was produced as described[51], with the following modifications. Rabies culture was performed in 2% serum at 35 °C with 3% CO_2 and two concentrating ultracentrifugation spins through sucrose were performed instead of one. Rabies starter viruses that contained either GFP, mCherry or ChR2 fused to mCherry (ChR2) were obtained from members of the Callaway lab[11,24]. AAV:G and rabies virus were mixed 4:1 immediately before injection. Injections were performed at P0 or P7 by anesthetizing pups on ice, then performing single injections of 0.3–1.5 µl (depending on the muscle) of virus into the muscle with a Hamilton syringe. Injections were performed through the skin, except for quadriceps injections that were performed using a small incision above the knee to reveal the muscle, and with a direct intramuscular injection. Small muscles (such as the TA and wrist flexors and extensors) were injected with low volumes (0.3–0.75 µl) using a needle with a small tip and a 30° bevel, whereas larger muscles were injected with 0.5–1.5 µl using a needle with a larger tip. Intraspinal injections of RabΔG:ChR2 were performed on P3 or P4 mice, anesthetized on ice, following a small unilateral laminectomy, and using a fine glass needle and a picospritzer to deliver 0.25 µl of virus into L4/L5. Animals were analyzed at P6–P8. Cortical injections of AAV2/1 containing *CAG:Cre-iRES-EGFP* (at a titer of 5×10^{13} genome copies/ml) were performed using a fine glass needle and a picospritzer to deliver 0.25 µl of virus 0.6 mm lateral to bregma at a depth of 0.4–0.45 mm from the surface of the caudal motor cortex[37,52].

Capsaicin treatment. P8 animals were given two small injections in the right heel of 0.1% capsaicin in ethanol, and killed and perfused after a 1.5 h survival time.

Tissue processing, *in situ* hybridization, immunohistochemistry and cell quantification. Perfused spinal cords were isolated and immersion-fixed for an additional 1 h, washed in PBS, washed in 30% sucrose and embedded in O.C.T. compound. Cryosections were cut at 30 µm for *in situ* hybridization and at 50 µm for immunohistochemistry. *In situ* probes (vGlut2, Gad65 and Gad67) were provided by Q. Ma[53] (Harvard Medical School). The following primary antibodies were used: rabbit anti-parvalbumin (Swant PV25, 1:1,000), rabbit anti-PSD95 (Invitrogen 51-6900, 1:500), guinea pig anti-vGlut1 (Millipore AB5905, 1:5,000), rabbit anti–c-fos (Santa Cruz sc-52, 1:2,000), rabbit anti-Pax2 (Invitrogen 716000, 1:1,000), rabbit anti-Tlx3 (provided by C. Birchmeier, Max Delbruck Center for Molecular Medicine), rabbit anti-Tcfap2β (Santa Cruz sc-8976, 1:500) and mouse anti-Satb1/2 (Abcam 51502, 1:500). In some cases, directly conjugated rabbit anti-Tcfap2β antibody was used, prepared with Apex antibody labeling kit (Invitrogen). Images were taken on a confocal microscope and are presented as *z*-projections unless otherwise noted. To count cells for location and marker positivity, all spinal cords were included that had at least 15 neurons in at least one 50 µm section, a minimum criteria for sufficient efficiency of trans-synaptic spread. High magnification images of synaptic contacts were taken with a 60× SC objective (Olympus) and spatially oversampled ≥twofold. To confirm synaptic contacts, double or triple co-localized pixels were analyzed with the ImageJ colocalization plugin. Only 8-bit pixel intensities ≥50 were considered for analysis. All averages were calculated with an s.d. Whole-cord reconstructions of transynaptic labeling were performed in ScaleA2 optically cleared intact spinal cords with a two-photon microscope and a 20× objective (Olympus). Individual *z*-stacks covering ~500 µm × 500 µm were combined using the pairwise stitching plugin for ImageJ. Three-dimenstionally rendered versions of confocal/two-photon *z*-stacks were generated with FluoRender.

Optical stimulation and electrophysiology. Animals were injected at P0 with ChR2-mCherry rabies virus, together with AAV:G. At P8, spinal cords were isolated in cold oxygenated dissection ACSF (128 mM NaCl; 4 mM KCl; 21 mM $NaHCO_3$; 0.5 mM NaH_2PO_4; 3 mM $MgSO_4$; 30 mM D-glucose; and 1 mM $CaCl_2$), hemisected and transferred to oxygenated room temperature recording ACSF (128 mM NaCl; 4 mM KCl; 21 mM $NaHCO_3$; 0.5 mM NaH_2PO_4; 1 mM $MgSO_4$; 30 mM D-glucose; and 2 mM $CaCl_2$) with the medial surface of the cord facing up and examined for trans-synaptic labeling (only cords with trans-synaptic labeling were analyzed). Suction electrodes were attached to the L2 and L4 or L5 ventral roots, and cords were then allowed to recover and equilibrate to room temperature for ~20 min. A 20× 1.0 numerical aperture (NA) objective was used to visualize cells and to deliver light to small groups of 2–10 cells. 50-ms light pulses were generated by a 200-W light source and high-speed shutter controlled by TTL signals from pclamp software. Latencies to motorneuron responses were measured from the onset of the stimulation, and the shutter opened completely within 5 ms of the stimulation window. Motorneuron responses were recorded with a multiclamp 700B amplifier and filtered at 300 Hz to 1 kHz. Stimulations proceeded from the caudal end of the lumbar cord, at ~500-µm intervals to the lower thoracic cord, usually covering ~3 mm. In intracord-injected nonspecific interneuron experiments, stimulations were also performed at three different dorsal-ventral locations, and the analysis presented here was performed on the ventral stimulation sites. Data were analyzed offline with clampfit and igor pro software. After recording, cords were immersion-fixed and sectioned to analyze the extent and pattern of neuron labeling and the morphology of labeled cells. Extracellular recordings from the MSE white matter were conducted with ~1-MΩ glass pipettes filled with ACSF placed in the vicinity of directly visualized *RabΔG:ChR2-Cherry*–labeled MSE axons in the cornu-commisuralis of Marie. We found that optical stimulation first evoked local action potentials within the cornu-commisuralis of Marie 11.7 ± 0.8 ms after the onset of light exposure over MSE and that the conduction velocity was 0.95 ± 0.3 ms/mm, or ~2.9 ms between L2 and L5 spinal segments ($n = 4$ spinal cords, **Supplementary Fig. 10**).

Statistical analysis general comments. No statistical methods were used to predetermine sample sizes, but our sample sizes are similar to those generally used in the field. Data collection and analysis were not performed blind to the conditions of the experiments. A normal q-q plot was used to test for normal distribution of the ChR2-evoked motor response data. All cell and synaptic contact counts are presented as means and s.d.

Statistical analysis of reliability of dual L2/L5 responses. Reliable dual-root response was defined as the percentage of locations in a given sample in which all trials produced L2 and L5 responses. Sample means were compared between MSE and nonspecific groups with a *t*-test.

Statistical analysis of principal component analysis (PCA). We used PCA to look for relationships between the summary metrics from each stimulation location: mean latency, latency s.d., response ratio, response pattern similarity (see below), dual root response ratio and rostral-caudal stimulation location. Location summary metrics were arranged in a table with metrics in columns. Columns were standardized and PCA was applied. A cutoff for component significance was established by Monte Carlo simulation of PCA applied to Gaussian noise of the same dimension and variance properties as the standardized metrics table. The 95th percentile of each principal component's variance from all Monte Carlo trials was used as a significance threshold. This revealed a single significant principal component (PC1), which strongly loaded mean latency, latency s.d., response pattern similarity, response ratio and dual root response ratio. The directions of the loadings suggested this component summarized response reliability (low latency s.d., high pattern similarity, high response ratio and high dual root response ratio). The standardized data were projected onto PC1 and averaged per sample. Sample means were compared between MSE and nonspecific groups at corresponding roots using a *t*-test.

Statistical analysis of response pattern similarity. Ventral root recordings were imported into the program R for analysis. Recordings were high-pass filtered at 100 Hz with a Butterworth filter and convolved with a typical 1-ms spike pattern to accentuate neuronal spikes over noise. High pass–filtered versions were rectified and convolved versions were analyzed to estimate locations of

doi:10.1038/nn.3675

significant neuronal spiking. The 95th percentile of convolution noise peaks before the stimulation was used as a simple height threshold for the data after the onset of the stimulation at each recording. Any points passing the height threshold in the convolved signal represent points in the raw signal where the 1-ms spike pattern was strongly associated. Those points were extracted from the high-passed signal, and all other points were set to zero. Finally the thresholded signal was clipped to 104 ms starting from the response onset minus 4 ms.

The responses were evaluated for consistency in pattern at each stimulation location. To avoid overlap with the response ratio metric, we only analyzed the trials that produced responses. Pattern similarity between any pair of responses was defined as the average of the 0-lag cross-correlation and the peak cross-correlation within a 4-ms window of either positive or negative lag. If there were no peaks in the cross-correlation spectrum then only the 0-lag value was used. Only positive values were considered valid. This metric allowed for the possibility that activity was not perfectly aligned between trials while still having an overall general similarity. For each stimulation location all pairwise similarities were averaged producing a single metric.

Statistical analysis of latency and location analysis. Mean latencies for L2 and L5 per stimulation location were pooled from all samples and plotted versus their corresponding rostral-caudal stimulation locations. L2 and L5 points were fit separately with a linear model. The slope of the linear fit was interpreted as the average change in latency versus change in rostral-caudal location. 95% confidence intervals of the slopes were generated by bootstrap resampling. Each bootstrap sample of latency versus location values was fit with a linear model, and the slope was recorded for 1,000 trials. The 2.5th and 97.5th percentiles of the bootstrap distribution defined the 95% confidence interval of average slope. The calculated conduction delay of 0.96 ms/mm latency rate of change was lower than the low end of the 95% confidence intervals, indicating that the L2 and L5 slopes were significantly higher than 0.96 ms/mm at $P < 0.05$.

51. Wickersham, I.R., Sullivan, H.A. & Seung, H.S. Production of glycoprotein-deleted rabies viruses for monosynaptic tracing and high-level gene expression in neurons. *Nat. Protoc.* **5**, 595–606 (2010).
52. Joshi, P.S. *et al.* Bhlhb5 regulates the postmitotic acquisition of area identities in layers II–V of the developing neocortex. *Neuron* **60**, 258–272 (2008).
53. Cheng, L. *et al.* Tlx3 and Tlx1 are post-mitotic selector genes determining glutamatergic over GABAergic cell fates. *Nat. Neurosci.* **7**, 510–517 (2004).